Available online at www.sciencedirect.com
SCIENCE DIRECT
Journal of Power Sources 158 (2006) 497–503
JOURNAL OF POWER SOURCES
www.elsevier.com/locate/jpowsour

Comparison of conversion and deposit formation of ethanol and butane under SOFC conditions

Gaurav K. Gupta [a], Anthony M. Dean [a,*], Kipyung Ahn [b], Raymond J. Gorte [b]

[a] *Chemical Engineering Department, Colorado School of Mines, 1613 Illinois Street, Golden, CO 80401, USA*
[b] *Chemical and Biomolecular Engineering, University of Pennsylvania, 220 South 33rd Street, Philadelphia, PA 19104-6393, USA*

Received 23 August 2005; received in revised form 24 September 2005; accepted 27 September 2005
Available online 14 November 2005

Abstract

This paper explores the gas-phase kinetics of butane and ethanol conversion as well as the propensity for molecular-weight growth and deposit formation in the non-catalytic regions of a solid oxide fuel cell (SOFC). Experiments are done where the fuel flows through a quartz reactor heated by a furnace. The primary observables are the extent of fuel conversion and the amount of deposit formed on a YSZ disk placed at the end of the furnace. Experiments are performed at 700, 750 and 800 °C. The residence times in the hot zone varied from 2 to 4 s. Ethanol is more reactive than butane, and almost all the ethanol is reacted at 750 °C whereas butane is completely reacted at 800 °C. Deposit formation is much larger for butane. These results are compared to predictions of a detailed kinetic model. Model predictions for the extent of fuel conversion and molecular-weight growth are in good agreement with the data for both fuels. Butane is predicted to be converted to the lighter hydrocarbons methane, ethylene, propylene and ethane. Hydrogen is also a significant product, especially at higher temperatures. For ethanol, the product distribution is different with lower amounts of hydrocarbons while substantial quantities of water, ethylene, CO and H_2 are predicted. In ethanol pyrolysis there is no significant production of species with more than two carbon atoms, whereas propylene production is significant in butane pyrolysis. Modeling results suggest this is a major reason for increased deposit formation with butane. Equilibrium calculations demonstrate that both the butane and ethanol systems are far removed from equilibrium.

Keywords: Ethanol ; Butane ; Gas-phase kinetics ; Conversion ; Deposits ; Pyrolysis

1. Introduction

A substantial advantage of solid oxide fuel cells (SOFC) is the ability to utilize hydrocarbons, although in practice measures must be taken to inhibit formation of carbon deposits [1–12].One approach to avoid deposit formation is to convert the fuel prior to the SOFC to a mixture of CO, H_2, CO_2, H_2O and perhaps CH_4 by steam reforming or catalytic partial oxidation (CPOX) [13,14]. A second approach is to add steam or air to the fuel and allow “internal reforming" within the SOFC anode [11,15,16]. Finally, if the anode materials are chosen so as to avoid catalysts that promote carbon formation, it may be possible oxidize hydrocarbons directly without addition of steam or O_2. For the second and third approaches, depending on the system design of the SOFC, inlet fuel mixtures can be exposed to high temperatures within flow-distribution networks before entering the membrane electrode assembly region. In this high-temperature environment, one might anticipate substantial gas-phase reactions of the fuel prior to either catalytic reactions within the porous anode or electrochemical oxidation at the three-phase boundary. Such reactions have the potential to significantly affect SOFC performance. First, the parent hydrocarbon can be converted to other species. Thus the species available for both catalytic conversion within the porous anode and subsequent electrochemical oxidation could have significantly different reactivity than the hydrocarbon being fed to the cell which could effect the fuel cell performance [17]. Second, the fuel might react to form deposits.

There are two mechanisms that exist at high temperatures for carbon deposition [9,18]. First, carbon can be formed as a result of reactions over a catalyst. This process has been very well studied over Ni, Fe and Co [19,20]. The mechanism on each of these metals involves deposition of a carbon source onto

* Corresponding author.
E-mail address: amdean@mines.edu (A.M. Dean).

0378-7753/$ – see front matter © 2005 Elsevier B.V. All rights reserved.
doi:10.1016/j.jpowsour.2005.09.036

the metal surface, dissolution of the carbon into the bulk of the metal, and finally precipitation of carbon as a graphite fiber at some surface of the metal particle. Second, reactions in the gas channels can lead to the production of higher-molecular weight species, e.g., aromatics, which can be deposit precursors [17]. These reactions are most important for hydrocarbons larger than methane and are usually initiated by C–C bond scission at high temperatures. We focus on the deposits formed via gas-phase reactions.

In this context, it is essential to characterize the gas-phase kinetics of hydrocarbon fuels and to understand how such reactions can influence the fuel conversion and deposit formation within flow-distribution networks before entering the active regions of the fuel cell. To explore the effect of gas-phase kinetics on extent of fuel conversion and deposit formation, pyrolysis experiments are done using butane and ethanol as fuels. Butane is chosen to represent a typical hydrocarbon fuel, while ethanol is important not only as a representative oxygenate, but also one that can be produced from renewable resources. Presence of the OH group in ethanol leads to a weakening of some C–H bonds, suggesting it might be more reactive than a hydrocarbon. Similarly, the product distribution is likely to be different. Thus the species available for both catalytic conversion within the porous anode and subsequent electrochemical oxidation could be much different than for butane. One might also expect that the presence of oxygen in ethanol will help in suppressing the deposits in the system.

A detailed reaction mechanism describing the pyrolysis kinetics of butane and ethanol is used to describe the extent of fuel conversion observed experimentally. These kinetic predictions agree well with the observations. We have also predicted the propensity for deposit formation for these systems by computing the amount of higher molecular weight species by summing the mass fractions of all species that contain five or more carbon atoms, designated as C_{5+}. It is demonstrated that there is a good correlation between the predicted amount of C_{5+} species and the mass fraction of deposit measured. The experimental results and the kinetic predictions show that the extent of deposits is much larger for butane. To understand the difference in the deposit formation for butane and ethanol, a rate analysis is done to identify the species leading to molecular weight growth for both the fuels. A comparison of the kinetic predictions to equilibrium calculations demonstrates that both systems are far removed from equilibrium. We also explore the role of steam in the feed streams since steam is frequently added to suppress catalytic deposit formation.

2. Experimental description and results

The pyrolysis experiments are performed in a 6.7 mm i.d. quartz flow reactor that is heated within a 25 cm furnace. The butane experiments used neat butane with a flow rate at room temperature of 32 $cm^3\,min^{-1}$, while ethanol was vaporized into a stream of helium. The vaporized ethanol flow rate was 26 $cm^3\,min^{-1}$ and the flow rate of He was 2.7 $cm^3\,min^{-1}$, resulting in an ethanol mole fraction of 0.90. Experiments are performed with the furnace set at three temperatures (700, 750 and 800 °C). In all cases, isothermal conditions are assumed. The residence times in the hot zone varied from 2 to 4 s. There are substantial increases in the flow velocity within the reactor, since there is an increase in the number of moles of gas as a result of the pyrolysis reactions. The relative tendency of these fuels to form deposits is determined by weighing the amount of deposit which collects on a porous YSZ slab placed near the furnace exit. The YSZ slabs, which were prepared by firing the mixture of YSZ powder (Tosoh, TZ-8Y) and graphite pore formers at 1550 °C for 4 h in air, had a porosity of 60%, with relatively uniform pores, 1.5 μm in diameter. The outlet gases from the quartz reactor were analyzed using an on-line gas chromatograph (Buck Scientific, model no. 8610) equipped with thermal conductivity detector and Hayesep Q packed column. Helium was used as the carrier gas. The experimental results are summarized in Table 1.

Table 1
Experimental data

	Temperature		
	700 °C	750 °C	800 °C
X_{exit}/X_{inlet} (butane)	0.22	0.06	0.01
X_{exit}/X_{inlet} (ethanol)	0.10	0.01	0
Deposit (g h^{-1}) (butane)	2.5×10^{-4}	3.0×10^{-3}	6.8×10^{-3}
Deposit (g h^{-1}) (ethanol)	0	7.5×10^{-5}	2.0×10^{-4}

It can be seen from Table 1 that both the fuels are essentially completely converted at 800 °C, with ethanol being more reactive than butane. Thus the species available for both catalytic conversion within the porous anode and subsequent electrochemical oxidation will be much different than the fuel being fed to the cell. It can also be seen that the extent of deposit formation is much larger for butane.

3. Kinetic model description

The detailed chemical mechanism used for this analysis includes detailed oxidation and pyrolysis kinetics for hydrocarbons up to C6. In addition, it includes the molecular weight growth reactions for polyaromatic hydrocarbons (PAH) formation via the hydrogen-abstraction-acetylene-addition mechanism of Frenklach and Warnatz [21]. The mechanism involves about 350 species and over 3450 reactions and has been validated for butane pyrolysis [17]. The mechanism has been also validated for methane pyrolysis and oxidation [22]. This mechanism was modified in several ways for the current set of calculations. We included several additional reactions involving ethanol. The most important are the two channels for ethanol dissociation:

$$C_2H_5OH \rightleftharpoons C_2H_4 + H_2O, \quad (1)$$

$$C_2H_5OH \rightleftharpoons CH_3 + CH_2OH. \quad (2)$$

Li et al. [23] have done ethanol pyrolysis experiments at 1.7–3.0 atm and 1045–1080 K using a variable pressure flow reactor. They have experimentally determined the rate constant k_1 of the molecular decomposition reaction (1) [the dominant reaction]. They measured C_2H_5OH and C_2H_4 concentrations to calculate the rate constant of reaction (1) at 3 atm according to the standard

Table 2
Comparison of the rate constant of the reaction $C_2H_5OH \rightleftharpoons C_2H_4 + H_2O$ reported by Li et al., predicted by RRKM [23] with CHEMDIS (using both MSC and ME) [24] calculations over a range of pressures and temperatures

P (atm)	$k_{1\,RRKM/CHEMDIS}$ (700 °C)		$k_{1\,RRKM/CHEMDIS}$ (750 °C)		$k_{1\,RRKM/CHEMDIS}$ (800 °C)	
	MSC	ME	MSC	ME	MSC	ME
0.01	0.96	0.95	1.02	1.00	1.04	1.01
0.1	1.05	1.02	1.13	1.09	1.17	1.11
1	1.05	1.04	1.12	1.11	1.16	1.14
10	1.05	1.02	1.10	1.06	1.13	1.09
100	1.00	0.98	1.02	1.00	1.03	1.01

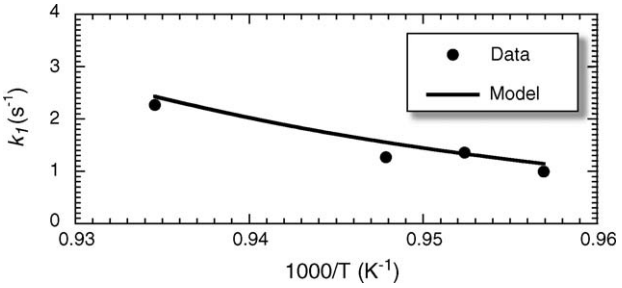

Fig. 1. Comparison of the rate constant of the reaction $C_2H_5OH \rightleftharpoons C_2H_4 + H_2O$ measured in the flow reactor experiments [23] with the CHEMDIS [24] calculations. Initial conditions used in the experiments were $P = 3.0$ atm, $C_2H_5OH = 0.12\%$ toluene ($C_6H_5CH_3$) = 0.12%, $O_2 = 35$ ppm with balance N_2.

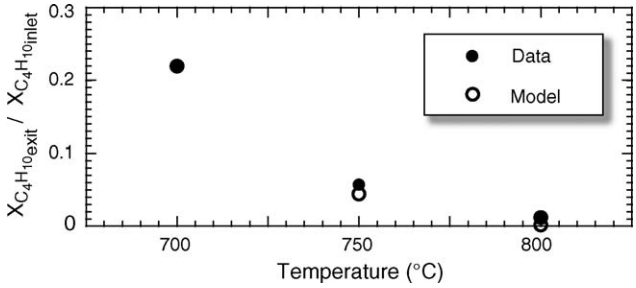

Fig. 2. Comparison of the ratio of exit to inlet mole fraction of butane observed experimentally with the model predictions as a function of temperature. (The butane level of conversion at 700 °C in the model is matched to the data. The residence times in the hot zone varied from 2.2 to 3.0 s.)

rate equation:

$$\frac{d[C_2H_4]}{dt} = k_1 \cdot [C_2H_5OH], \quad (3)$$

where $[X]$ is the concentration of species X and t is the reaction time. The experimentally determined rate constant k_1 is presented in Fig. 1. Initial conditions used in the experiments were $P = 3.0$ atm, $C_2H_5OH = 0.12\%$, toluene ($C_6H_5CH_3$) = 0.12%, $O_2 = 35$ ppm with balance N_2. The purpose of adding $C_6H_5CH_3$ is to act as a radical trap to prohibit significant reactions of ethanol with the reactive radicals (CH_3, H, OH, and so on) that would otherwise result from the decomposition products. As a consequence, approximately 92% of the total C_2H_4 formed under these conditions is predicted to be generated by the H_2O elimination reaction (1). As a result, the rate constant k_1 can be determined directly from the measurements of the ethylene formation rate and ethanol concentration.

Li et al. [23] have not reported the expression for k_1 at 3 atm. In order to compare the value of k_1 at 3 atm we used k_∞ for reaction (1) reported by Li and coworkers and calculated the expression for k_1 at 3 atm using CHEMDIS [24]. CHEMDIS uses a three-frequency version of QRRK theory and either a modified strong-collision (MSC) or master equation (ME) approximation to estimate collisional stabilization. Fig. 1 illustrates a comparison between the model predictions using MSC and the measured rate constant k_1 over a range of temperatures. It can be seen that the model accurately captures the observed behavior.

The multichannel unimolecular decomposition of ethanol was calculated using RRKM/master equation calculations by Li et al. [23] over a wide range of pressures (0.01–100 atm). We also calculated the k_1 at those pressures with CHEMDIS. Table 2 lists the ratio of the k_1 value calculated by Li et al. to that calculated by CHEMDIS using both MSC and ME over a range of pressures and temperatures. It can be seen that values of k_1 calculated by CHEMDIS (using both MSC and ME) are in excellent agreement with the values reported by Li et al. For the current kinetic model values of k_1 and k_2 at 1 atm are required. We used the CHEMDIS values, computed using the MSC approximation at 1 atm, in our mechanism.

Second, we included the hydrogen abstractions of $H_2C^\bullet CH_2OH$, $H_3CC^\bullet HOH$ and $CH_3CH_2O^\bullet$ from ethanol itself. These are indirect pathways for isomerization of these radicals. Hydrogen abstraction reactions from ethanol by other radicals were already included in the earlier mechanism. All reactions in the mechanism are reversible, with the reverse rate coefficients computed from the calculated temperature-dependent equilibrium constants. [1]

4. Model comparisons to observations

4.1. Extent of conversion and deposit formation

Calculations are done with pure C_4H_{10} and a C_2H_5OH/He mixture at three different temperatures (700, 750 and 800 °C) using CHEMKIN [25] and assuming plug flow. Due to the uncertainties in the temperature-distance profiles within the furnace, especially near the entrance and exit, we adjusted the distance in the model to achieve the measured conversion of butane at 700 °C. This distance (25.1 cm) can be compared to the nominal reactor length of 25 cm. This distance was then kept constant for all other calculations for both butane and ethanol.

Fig. 2 summarizes the comparison between the observed and the predicted level of conversion of butane at different tem-

[1] The mechanism and the associated thermodynamic database are available upon request.

peratures. It can be seen that the model captures the butane conversion very well over the range of temperatures. It can also be seen that, even at 700 °C, most of the butane has reacted.

Similarly Fig. 3 compares the extent of conversion of ethanol observed in the experiments to that predicted. It can be seen that the model captures the extent of ethanol conversion over the range of temperatures. Ethanol is more reactive than butane; at 700 °C and a residence time of 3.0 s 87% is reacted, as compared to 78% for butane (Fig. 2).

Sheng and Dean [17] suggested that one could correlate the onset of observed deposit formation with the predicted total mole fraction of species with molecular weight larger than butane (C_{5+}). Although this is clearly an approximation, these higher molecular weight species are typically cyclic unsaturated compounds that are the likely precursors of polynuclear aromatic hydrocarbons. Moreover, formation of the first aromatic ring is generally considered to be the rate-limiting step in soot formation.

To make a more direct connection between the predictions and observed deposit formation, we need to consider the cumulative effect of flowing the gas for a specified time interval. In this manner, an upper limit to deposit formation can be obtained by computing the total mass fraction of C_{5+} that exits the reactor. (This is an upper limit since not all the C_{5+} produced will form deposits and not all the deposits will be collected on the YSZ disk.) To compare the observed deposit to the predicted C_{5+} mass fraction, we calculate the fraction of fuel that is deposited by using the data in Table 1 with the inlet flow rate and the specified time interval over which the deposits were formed. To relate the calculated C_{5+} mass fractions to the fraction of the fuel going to deposits we use a normalization factor (F):

$$\text{Predicted deposit (mass fraction)} = F \cdot C_{5+}\ \text{(mass fraction)}.$$

With $F = 0.02$, we obtain reasonable agreement between predicted and observed deposit amounts for both fuels, as shown in Fig. 4. Of particular interest is that the kinetic model captures the strong temperature dependence that is observed for butane. However the model predicts slightly stronger temperature dependence than is observed for ethanol. Especially encouraging is that the same normalization factor applies reasonably well to both fuels.

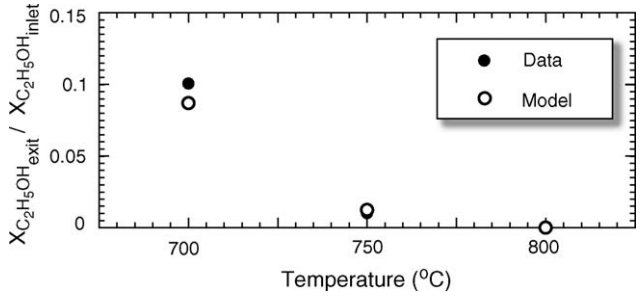

Fig. 3. Comparison of the ratio of exit to inlet mole fraction of ethanol observed experimentally with the model predictions as a function of temperature. (The residence times in the hot zone varied from 2.5 to 4.4 s.)

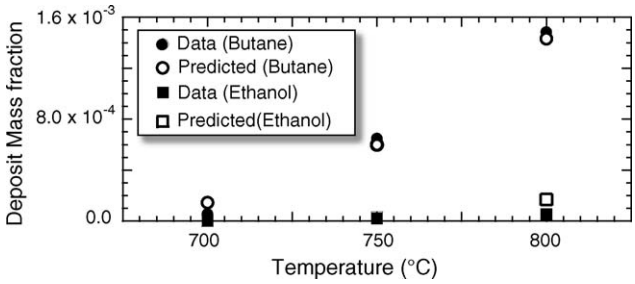

Fig. 4. Comparison of experimentally observed deposit mass fraction with the model predictions as a function of temperature for butane and ethanol.

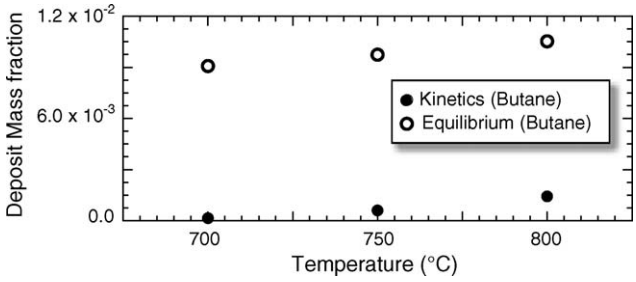

Fig. 5. Comparison of kinetic predictions of deposit mass fraction for butane to the equilibrium values as a function of temperature.

4.2. Kinetics versus equilibrium

We also predicted the mass fraction of deposits at equilibrium using the minimization of free energy approach [25]. In the equilibrium calculations reported below, we do not include graphite as a possible product. One expects that graphite formation from gas-phase reactions would be very slow. The mechanism for molecular-weight growth leads to production of polyaromatic hydrocarbon (PAH) molecules, which contain appreciable H. To form graphite all the H atoms must be removed via reactions. Indeed, it has been reported that deposits consists of PAH [9]. Using the same normalization factor described above, the equilibrium deposit mass fraction is predicted for both the fuels. Fig. 5 compares the deposit mass fraction for butane predicted kinetically to the equilibrium result at different temperatures. It can be seen that system is far from equilibrium, with much less deposit observed than expected at equilibrium.

Similarly Fig. 6 shows a similar comparison for ethanol. It can be seen that the system is close to equilibrium at lower temperatures. However, at 800 °C the observed level of deposits is much

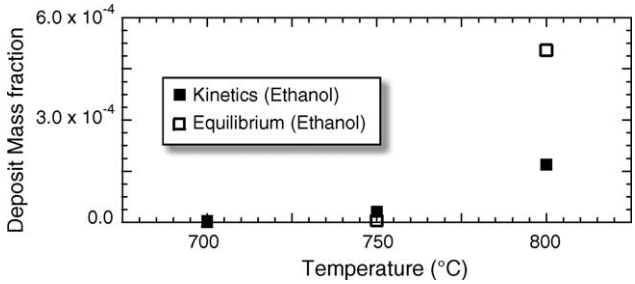

Fig. 6. Comparison of kinetic predictions of deposit mass fraction for ethanol to the equilibrium values as a function of temperature.

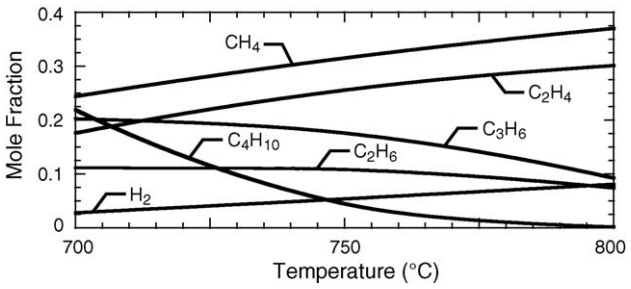

Fig. 7. Predicted major species at the end of the hot zone as a function of temperature for butane pyrolysis.

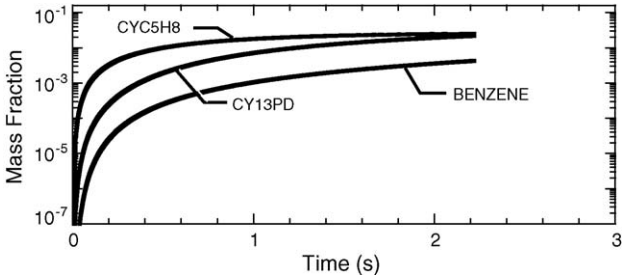

Fig. 9. Mole fractions of major species contributing to C_{5+} as a function of residence time at 800 °C for butane.

lower than predicted at equilibrium. We have also calculated the fuel conversion at equilibrium and found that both the fuels are completely converted to other species even at 700 °C. Thus both conversion and deposit formation are kinetically controlled. Additional calculations that allowed formation of graphite indicated even larger differences to the measured deposits.

4.3. Model predictions for species distribution

Fig. 7 summarizes the predictions for the distribution of major species as a function of temperature for butane pyrolysis. It can be seen that by 800 °C butane (C_4H_{10}) is completely converted and substantial quantities of the lighter hydrocarbons methane (CH_4), ethylene (C_2H_4), propylene (C_3H_6) and ethane (C_2H_6) are produced. H_2 is also a significant product, especially at higher temperatures.

Fig. 8 summarizes the predictions of the major species as a function of temperature for ethanol pyrolysis. Less that 1% of the ethanol remains at 750 °C. The product distribution is significantly different from butane, with substantial quantities of water and ethylene directly produced by the primary ethanol dissociation reaction (Rxn 1). As compared to butane pyrolysis (Fig. 7) the amounts of CH_4 and C_2H_6 are significantly lower in ethanol pyrolysis, while C_2H_4 is somewhat lower. Also there is no significant production of species with more than two carbon atoms, whereas propylene production is significant in butane pyrolysis. Ethanol pyrolysis also produces relatively large amounts of CO and H_2.

To understand the difference in the C_{5+} production for butane and ethanol, we identified the dominant C_{5+} species for the two cases and plotted these mole fractions at 800 °C in Figs. 9 and 10 for butane and ethanol, respectively. (In these figures, a residence time of 2.2 s corresponds to the end of the heated reactor for butane pyrolysis, while the corresponding time for ethanol pyrolysis is 2.5 s.)

As can be seen from the figures, the major molecular weight growth species for both fuels are the same, although their relative importance is different for the two fuels. The cyclic C5 species cyclopentene (CYC5H8) and 1,3 cyclopentadiene (CY13PD) are most important for butane, while benzene is most important for ethanol. Note that the cyclic C5 species are present in much lower amounts for the ethanol case.

A rate analysis is done at 800 °C for these three species for both butane and ethanol to identify the important reaction pathways. As expected from the mole fraction plot, the rate of production of 1,3 cyclopentadiene is much faster for butane. The important pathways include:

$$C_3H_5 + C_2H_2 \rightarrow C_5H_6(1,3\,\text{cyclopentadiene}) + H, \quad (4)$$

$$C_3H_3 + C_2H_2 \rightarrow C_5H_5(\text{cyclopentadienyl radical}), \quad (5)$$

$$C_5H_5(\text{cyclopentadienyl radical}) + RH \rightarrow C_5H_6(1,3\,\text{cyclopentadiene}) + \dot{R}. \quad (6)$$

For cyclopentene, one reaction dominates:

$$C_3H_5 + C_2H_4 \rightarrow C_5H_8(\text{cyclopentene}) + H. \quad (7)$$

Cylcopentene is then converted to 1,3 cyclopendiene:

$$C_5H_8(\text{cyclopentene}) + \dot{R} \rightarrow C_5H_7(\text{cyclopentenyl radical}) + RH, \quad (8)$$

$$C_5H_7(\text{cyclopentenyl radical}) \rightarrow C_5H_6(1,3\,\text{cyclopendiene}) + H. \quad (9)$$

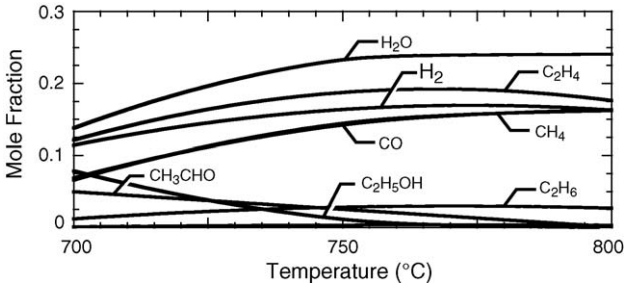

Fig. 8. Predicted major species at the end of the hot zone as a function of temperature for ethanol pyrolysis in helium.

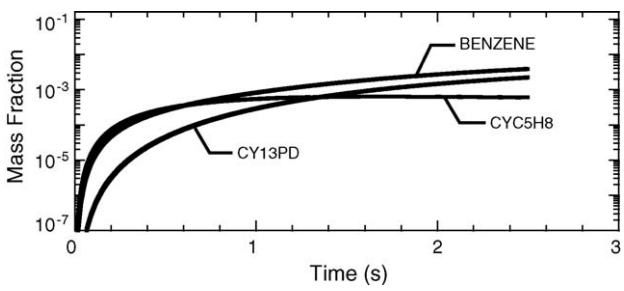

Fig. 10. Mole fractions of major species contributing to C_{5+} as a function of residence time at 800 °C for ethanol.

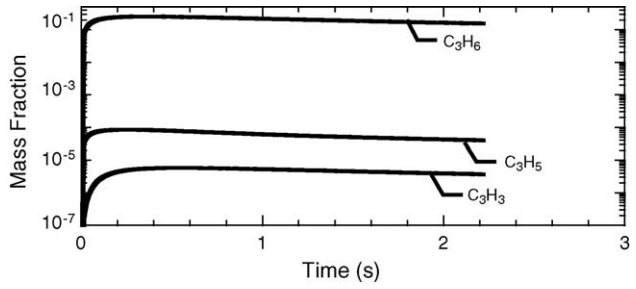

Fig. 11. Predicted mole fractions of C_3H_5, C_3H_3 and C_3H_6 at 800 °C for butane.

Both cyclic C5 species are formed by addition of resonantly stabilized C3 radicals (allyl (C_3H_5) and propargyl (C_3H_3) to the unsaturated C2 molecules. Moreover, C_3H_5 and C_3H_3 radicals are both formed from propylene (C_3H_6). In this sense, it can be said that it is that production of the C5 deposit precursors requires reasonably high concentrations of both C2 and C3 unsaturated molecules.

When we compared the rates for production of benzene for butane and ethanol we found that in both cases benzene comes from following reaction pathway:

$$C_2H_3 + C_2H_4 \rightarrow C_4H_6(1,3\ \text{butadiene}) + H, \quad (10)$$

$$C_2H_3 + C_4H_6 \rightarrow C_6H_8(\text{cyclohexene}) + H, \quad (11)$$

$$C_6H_8 + R^{\cdot} \rightarrow C_6H_7(\text{cyclohexadienyl radical}) + RH, \quad (12)$$

$$C_6H_7(\text{cyclohexadienyl radical}) \rightarrow C_6H_6(\text{benzene}) + H. \quad (13)$$

Thus, only the C2 unsaturates participate in a major way for benzene production. It can be seen from Figs. 9 and 10 that the benzene mass fraction is similar for the two fuels. The mole fractions of C_2H_4 are comparable for both fuels, as seen from Figs. 7 and 8. The predicted C_2H_2 mole fractions are also comparable for the two fuels but two orders of magnitude less than C_2H_4. Thus the similar mole fractions of C2 unsaturates lead to similar rates of benzene production for the two fuels.

These results suggest that the difference in the rate of formation of deposit precursors for these two fuels is related to different mole fractions of the C3 unsaturated molecules produced during pyrolysis. The model predictions indicated much lower concentrations of propylene in the ethanol system. We expect this lower value to result in much lower mole fractions of allyl and propargyl – the radicals responsible for formation of the cyclic C5 species. We compare the predicted mole fractions in Figs. 11 and 12. As expected, we see much lower mole fractions of three radicals for the ethanol case, and this leads to the much lower propensity for deposit formation for ethanol.

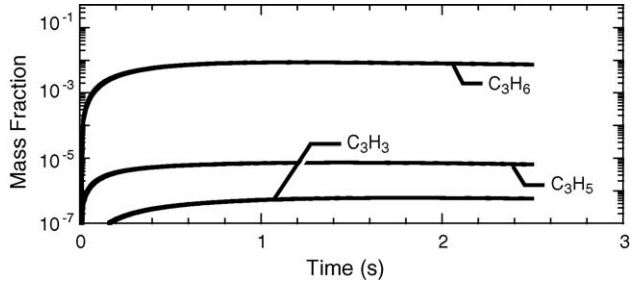

Fig. 12. Predicted mole fractions of C_3H_5, C_3H_3 and C_3H_6 at 800 °C for ethanol.

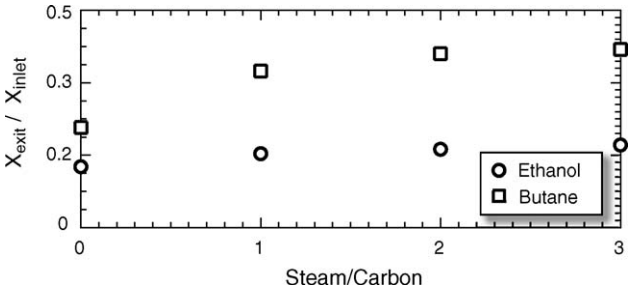

Fig. 13. Predicted ratio of exit to inlet mole fraction of butane and ethanol at 700 °C as a function of steam to carbon ratio.

5. Model predictions of the impact of steam dilution

It is often desirable to premix steam or air with the hydrocarbon fuel to inhibit catalytic deposit formation. To see the effect of steam dilution on the gas-phase reactions, we varied the steam to carbon ratio for both the fuels at 700°C.

Fig. 13 shows the effect of steam dilution on the fuel conversion at 700 °C. It can be seen that even in the presence of large amounts of steam the level of conversion is only slightly less than the system without any added steam for both fuels. To ascertain whether H_2O was acting simply as a diluent or as a reactant, N_2 was substituted for steam. The results were very similar, indicating the primary effect of steam addition on the gas-phase reactions is dilution. (Of course the presence of H_2O will enhance catalytic reactions within the anode, providing a reforming catalyst is present.)

6. Summary

Experiments on butane and ethanol pyrolysis are performed at three different temperatures (700, 750 and 800 °C). A detailed reaction mechanism is used to describe the pyrolysis kinetics. The kinetic model accurately captures the extent of fuel conversion over the temperature range for both fuels. The experimental results illustrate some significant differences between butane and ethanol pyrolysis, especially in terms of deposit formation (much lower with ethanol as compared to butane). It is demonstrated that there is a good correlation between the predicted amount of C_{5+} species and the mass fraction of deposit formed. Model predictions for the extent of molecular-weight growth are in reasonable agreement with the data over the range of temperatures for both fuels. The strong temperature dependence of deposit formation can be traced to the rapid increase of the gas-phase molecular weight growth reactions with temperature. These results also reinforce our earlier finding that one might expect to see substantial gas-phase conversion of the parent fuel within the gas channels of a SOFC, even with a large amount of added steam. The kinetic model predicts that, even at 700 °C, most of the fuel will be converted within a few seconds residence time in the channel. The kinetic predictions showed that butane is completely converted to lighter hydrocarbons CH_4, C_2H_4, C_3H_6

and C_2H_6 at 800 °C. H_2 is also a significant product, especially at higher temperatures. The ethanol product distribution is significantly different from butane. As compared to butane pyrolysis, the amount of hydrocarbons are lower in ethanol pyrolysis. Ethanol pyrolysis also produces relatively large amounts of CO and H_2. Thus the species available for both catalytic conversion within the porous anode and subsequent electrochemical oxidation are much different than the fuel being fed to the cell. The model predictions indicated much lower concentration of C_3H_6 in the ethanol system. The lower value of C_3H_6 results in much lower mole fractions of C_3H_5 and C_3H_3 – the radicals responsible for formation of the cyclic C5 species. Lower mole fractions of these radicals for the ethanol case leads to the much lower propensity for deposit formation for ethanol. It was also found that H_2O has little effect on the pyrolysis reactions under these conditions. A comparison to equilibrium predictions show that a kinetic model is essential to predict levels of conversion, product distribution and deposit formation.

Acknowledgements

This research was supported by Office of Naval Research, Grant N00014-02-1-0665 (Colorado School of Mines) and Grant N00014-03-1-0602 (University of Pennsylvania).

References

[1] A. Weber, B. Sauer, A.C. Müller, D. Herbstritt, E. Ivers-Tiffée, Oxidation of H_2, CO and methane in SOFCs with Ni/YSZ-cermet anodes, Solid State Ionics 152–153 (2002) 543–550.
[2] E.P. Murray, T. Tsai, S.A. Barnett, A direct-methane fuel cell with a ceria-based anode, Nature 400 (1999) 649–651.
[3] G.J. Saunders, K. Kendall, Reactions of hydrocarbons in small tubular SOFCs, J. Power Sources 106 (2002) 258–263.
[4] H. Kim, S. Park, J.M. Vohs, R.J. Gorte, Direct oxidation of liquid fuels in a solid oxide fuel cell, J. Electrochem. Soc. 148 (2001) A693–A695.
[5] J.B. Wang, J.-C. Jang, T.-J. Huang, Study of Ni-samaria-doped ceria anode for direct oxidation of methane in solid oxide fuel cells, J. Power Sources 122 (2003) 122–131.
[6] J. Liu, S.A. Barnett, Operation of anode-supported solid oxide fuel cells on methane and natural gas, Solid State Ionics 158 (2003) 11–16.
[7] K. Kendall, C.M. Finnerty, G. Saunders, J.T. Chung, Effects of dilution on methane entering an SOFC anode, J. Power Sources 106 (2002) 323–327.
[8] S.J.A. Livermore, J.W. Cotton, R.M. Ormerod, Fuel reforming and electrical performance studies in intermediate temperature ceria-gadolinia-based SOFCs, J. Power Sources 86 (2000) 411–416.
[9] S. McIntosh, H. He, S.-I. Lee, O. Costa-Nunes, V.V. Krishnan, J.M. Vohs, R.J. Gorte, An examination of carbonaceous deposits in direct-utilization SOFC anodes, J. Electrochem. Soc. 151 (2004) A604–A608.
[10] Y. Jiang, A.V. Virkar, A high performance anode-supported solid oxide fuel cell operating on direct alcohol, J. Electrochem. Soc. 148 (2001) A706–A709.
[11] Z. Zhan, J. Liu, S.A. Barnett, Operation of anode-supported solid oxide fuel cells on propane air fuel mixtures, Appl. Catal. A 262 (2004) 255–259.
[12] T. Kim, G. Liu, M. Boaro, S.-I. Lee, J.M. Vohs, R.J. Gorte, A study of carbon formation and prevention in hydrocarbon-fueled sofc, J. Power Sources, in press.
[13] C.T. Goralski, R.P. O'Connor, L.D. Schmidt, Modeling homogeneous and heterogeneous chemistry in the production of syngas from methane, Chem. Eng. Sci. 55 (2000) 1357–1370.
[14] J.-W. Snoeck, G.F. Froment, M. Fowles, Steam/CO_2 reforming of methane. Carbon formation and gasification on catalysts with various potassium contents, Ind. Eng. Chem. Res. 41 (2002) 3548–3556.
[15] S.H. Clarke, A.L. Dicks, K. Pointon, T.A. Smith, A. Swann, Catalytic aspects of the steam reforming of hydrocarbons in internal reforming fuel cells, Catal. Today 38 (1997) 411–423.
[16] F.A. Coutelieris, S. Douvartzides, P. Tsiakaras, The importance of the fuel choice on the efficiency of a solid oxide fuel cell system, J. Power Sources 123 (2003) 200–205.
[17] C.Y. Sheng, A.M. Dean, The importance of gas phase kinetics within the anode channel of a solid-oxide fuel cell, J. Phys. Chem. A 108 (2004) 3772–3783.
[18] S. McIntosh, R.J. Gorte, Direct hydrocarbon sofc, Chem. Rev. 104 (2004) 4845–4865.
[19] B. Monnerat, L. Kiwi-Minsker, A. Renken, Hydrogen production by catalytic cracking of methane over nickel gauze under periodic reactor operation, Chem. Eng. Sci. 56 (2001) 633–639.
[20] T. Zhang, M.D. Amiridis, Hydrogen production via the direct cracking of methane over silica-supported nickel catalysts, Appl. Catal. A 167 (1998) 161–172.
[21] M. Frenklach, J. Warnatz, Detailed modeling of PAH profiles in a sooting low-pressure acetylene flame, Combust. Sci. Tech. 51 (1987) 265–283.
[22] G.K. Gupta, E.S. Hecht, A.M. Dean, H. Zhu, R.J. Kee, Gas-phase reactions of methane and natural gas with air and steam in the non-catalytic channels of a solid-oxide fuel cell, J. Power Sources, in press.
[23] J. Li, A. Kazakov, F.L. Dryer, Experimental and numerical studies of ethanol decomposition reactions, J. Phys. Chem. A 108 (2004) 7671–7680.
[24] A.Y. Chang, J.W. Bozzelli, A.M. Dean, Kinetic analysis of complex chemical activation and unimolecular dissociation reactions using qrrk theory and the modified strong collision approximation, Zeitschrift für Physikalische Chemie 214 (2000) 1533–1568.
[25] R.J. Kee, F.M. Rupley, E. Meeks, J.A. Miller, CHEMKIN-III: a FORTRAN chemical kinetics package for the analysis of gas phase and plasma kinetics, technical report SAND96-8216, Sandia National Laboratories, 1996.